CHAPTER VI

BLOWN FILMS OF POLYPROPYLENE NANOCOMPOSITES: EMPHASIS ON MORPHOLOGICAL STUDY, CRYSTAL STRUCTURE, MECHANICAL AND THERMAL PROPERTIES

6.1 Abstract

The masterbatch of PP-clay nanocomposites consisting of MSBEN was prepared via the reactive extrusion process by using a plasma generator. Afterward, the masterbatch was further mixed with PP to obtain PP nanocomposites with 1 wt% of MSBEN. Finally, the nanocomposites were blown to a clear film for packaging application. The effects of contents of silver nanoparticles (5, 10, 15, 20 wt% in clay) on morphology, crystal structure, mechanical, and thermal properties were assessed. From the results, PP nanocomposites with 1 wt% of nanoclay were intercalated and partly exfoliated structures through the expansion of clay interlayers, observed by XRD. FE-SEM showed a good distribution and dispersion of modified clay in the PP matrix stemming from the double melt-mixing process. With respect to mechanical properties accordance to ASTM D882, the nanocomposite films demonstrated an increase in the Young's modulus implying the higher stiffness of materials arised from the advantages of a nanoscopic, high-surface-area filler. Conversely, the PP nanocomposite films showed the decrease in the tensile strength and % elongation at break comparable to neat PP film, resulting from certain inhomogeneous aggregates and some voids around dispersed phase. For DSC analysis, it was found that crystallization temperature, melting temperature, and % crystallinity had a tendency to increase as a result of nucleating effect from modified clay and silver nanoparticles. Surprisingly, at 2 wt% loss from TGA analysis, it was clearly shown that the PPS20BEN film exhibited higher thermal stability than that of neat PP film approximately 20 °C.

Keywords: Clay, Nanocomposites, Packaging, Polypropylene, Silver nanoparticles

6.2 Introduction

Polymer-clay nanocomposites have captured the attention of researchers with thanks to their remarkable properties (Maria *et al.*, 2006). Typically, addition of a few amount of clay (usually not exceeding 5 wt.%) (Azizi *et al.*, 2010) to polymer may enhance mechanical and thermal properties of nanocomposites originating from the platelet structure with high aspect ratio of clay in nano-scale dispersion (Sharma *et al.*, 2009). Polypropylene (PP), one of the major commodity plastics, is widely used in several engineering and biomedical applications. Among all thermoplastics, it offers best performance and low cost (Tang *et al.*, 2003). Bentonite is a member of smectite clay, which is a layered aluminium silicate with exchangeable cations and reactive OH groups on the surface. Since bentonite is hydrophilic, it is not compatible with most polymers and must be chemically modified to render its surface more hydrophobic (Ray and Okamoto, 2003).

With the advent of antimicrobial packaging, the incorporation of antimicrobial agents show promise as an effective way for the resistance of certain microorganisms in foods (Cooksey, 2005). Among metallic nanoparticles, silver nanoparticles manifest its wide ranges of application in various sections of life and industry. The silver is an effective antibacterial metal and non-toxic to animal cells but strongly toxic to bacteria, such as *Escherchia coli* (*E. coli*) (Ghosh and Ramamoorthy, 2010) and *Staphylococcus aureas* (El-Kheshen and Gad El-Rab, 2012), as well as highly toxic against fungi, such as *Candida albicans (C. albicans)*, *Saccharomyces cerevisiae (S. cerevisiae)* (Nasrollahi *et al.*, 2011), and *Colletotrichum* species (Lamsal *et al.*, 2011). Silver nanoparticles, particularly, have exhibited potemtial properties for antimicrobial agents in food packaging. Since silver nanoparticles can interrupt enzymatic activity of microbial cells, one of the crucial aims of addition of these silver nanoparticles is to promote the safety and prolong the shelf-life of meat products by lessening the rate of surface growth of specific microorganisms by direct contact of the packaging with the products (Appendini and Hotchkiss, 2002).

The objective of this chapter is to develop an antimicrobial agent-immobilized smart packaging film made of polypropylene based on nanotechnology.

Silver nanoparticles were synthesized into the interlayer of bentonite. After that, the silver nanoparticle-loaded bentonite was modified by organosilane prior to mixing. The masterbatch of PP-clay nanocomposites was prepared by plasma-based process. The masterbatch was mixed with PP to obtain 1 wt% of modified clay and then blown to produce a clear film. This chapter studied the effects of contents of silver nanoparticles (5, 10, 15, and 20 wt%) on morphology, mechanical and thermal properties of nanocomposite films.

6.3 Experimental Parts

6.3.1 Materials

Commercial polypropylene (PP) under trade name 2300K (MFI 4 g/10 min) supported from T.H.L. Industry Co., Ltd. was used as received. Commercial polypropylene (PP) under trade name NK 1126 (MFI 11 g/10 min) supported from T.H.L. Industry Co., Ltd. was used as received. Dicumyl peroxide (DCP), CAS NO. 80-43-3 was purchased from Aldrich and used as received. The commercial sodium activated bentonite Mac-Gel® (GRADE SAC), Na-BTN, with cationic exchange capacity (CEC) of 49.74 meq/100 g clay and surface area of 31.0 m^2/g, supplied by Thai Nippon Co., Ltd. Thailand, was purified before use. Silver (I) nitrate ($AgNO_3$), CAS NO. 7761-88-8, was purchased from Carlo Erba and used as received. Trisodium citrate dihydrate ($Na_3C_6H_5O_7$), CAS NO. 6132-04-3, was purchased from Carlo Erba and used as received. Absolute ethanol (C_2H_5OH), AR grade, CAS NO. 64-17-5, and glacial acetic acid (CH_3COOH), CAS NO. 64-19-7, were purchased from RCI Labscan and used as received, respectively

6.3.2 Preparation of Purified Clay

The sodium bentonite clay was first vigorously stirred into a deionized water at 700 rpm overnight by a mechanical stirrer. After that, the supernatant (swollen clay) was separated by centrifugation at 10,000 rpm for 15 minutes and lastly dried, sieved by mesh#400 and kept in a dessiccator before use.

6.3.3 Modification of Bentonite (BEN)

1.5 wt.% of MPS solution was prepared in 70 vol.% of ethanol ol aqueous solution pH 4 adjusted by glacial acetic acid and then stirred for 45 min of

hydrolysis to silanol. 50 g of bentonite were added respectively into MPS solution. The mixture was stirred at 110 °C for 24 hr. The plenty of absolute ethanol was used for the removal of excessive MPS during suction filtrating and the modified clay was finally dried at 80 °C in vacuum oven for 24 hr. The clay was pulverized by ball mill and then sieved by mesh#400 and kept in a desiccator prior to use.

6.3.4 Preparation of Silver Nanoparticle-Loaded Clay (SBEN)

50 g of purified bentonite were firstly stirred in $AgNO_3$ solution at room temperature overnight. The silver-ion clay was then reacted with $C_6H_5Na_3O_7 2H_2O$ at 1 : 3 molar ratio of $AgNO_3$ to $C_6H_5Na_3O_7 2H_2O$ at 90 °C for 20 min to obtain a silver nanoparticles clay (SBEN). The as-synthesized silver nanoparticle-loaded clay was measured their shape and size by a transmission electron microscope (TEM) as well as their crystal structure by an X-ray diffractometer (XRD).

6.3.5 Modification of Silver Nanoparticles-Loaded Clay (MSBEN)

The as-prepared silver nanoparticles-loaded bentonite (SBEN) was modified via silanation process. 1.5 wt.% of MPS solution was prepared in 70 vol.% of ethanol aqueous solution pH 4 adjusted by glacial acetic acid and then stirred for 45 min of hydrolysis to silanol. 50 g of the clay were added respectively into the MPS solution. The mixture was stirred at 110 °C for 24 hr. The plenty of absolute ethanol was used for the removal of excessive MPS during suction filtrating and the modified clay was finally dried at 80 °C in vacuum oven for 24 hr. The clay was pulverized by ball mill and then sieved by mesh#400 and kept in a desiccator prior to use.

6.3.6 Preparation of Polypropylene-Modified Bentonite Masterbatch and Polypropylene-Modified Silver Nanoparticles-Loaded Bentonite Masterbatch via a Plasma-based Processing

Both the PP and modified clay (6.3.3) and PP and modified silver nanoparticles-loaded bentonite (6.3.5) were mixed in the co-rotating twin-screw extruder (Labtech types LTE-20-32 & LTE-20-40 screw diameter 20 mm) with L/D ratio 40:1. The operation temperature was carried out at 100, 180, 185.190, 190, 190, 190, 195, 200, and 200 °C from hopper to die, respectively and the screw speed at 10 rpm. During exiting die, the melt extrudate of each of the compounds was

immediately treated by the plasma generator (PT-1 PLASMA TREATER) operated at 6 kV, 10 kHz for 5 sec at the distance of 4 cm from its nozzle to the extrudate.

6.3.8 Preparation of Active Films

The masterbatch of PP-MBEN (PPC-PLASMA) or PP-MSBEN (6.3.5) was further mixed with PP pellet in the ratio of PP : modified clay = 99 : 1 wt% (each compounds containing 1 wt.% of modified clay) in the co-rotating twin-screw extruder (Labtech types LTE-20-32 & LTE-20-40 screw diameter 20 mm) with L/D ratio 40:1. The operation temperature was performed at 100, 180, 185,190, 195, 195, 195, 195, 200, and 200 °C from hopper to die, respectively and the screw speed at 30 rpm. Each of the nanocomposites was transformed into active films by using a Labtech (model LTE20-30) single-screw extruder with L/D = 40 (D = 20 mm and L = 800) and annual die with outer diameter of 70 mm and inner diameter of 68.5 mm. The operating temperature of blown film extrusion machine was operated in the range of 180 – 200 °C and the rotational screw speed was fixed at 60 rpm with the blow up ratio of 2 : 1.

6.3.9 Characterization

6.3.9.1 Field Emission-Scanning Electron Microscope (FE-SEM)

For the nanocomposite extrudates, the dispersion of bentonite in polymer matrix was determined by using an FE-SEM (HITACHI, S-4800) coupled with energy dispersive X-ray spectrometer (EDS). The selected samples were dipped and fractured in liquid nitrogen. Then the samples were sputtered with platinum before viewing under the FE-SEM/EDS operated at 20 kV with the magnifications of 1K and 4.5K.

In part of nanocomposite films, the cryogenic-fractured surface of cross-sectional area of the films was investigated by using an SEM (HITACHI, S-2500). The selected films were dipped and fractured in liquid nitrogen. The samples were then sputtered with platinum before viewing under an SEM operated at 15 kV with the magnification of 10K.

6.3.9.2 Universal Testing Machine – Lloyd

Tensile test of the active film (~ 30 μm in thickness) by blown film extrusion machine operated according to ASTM D882 was carried out by Lloyd

Universal Testing Machine. The specimen was cut in machine direction into rectangular shape with 100 x 100 mm. Crosshead speed is 50 mm/min.

6.3.9.3 Differential scanning calorimeter (DSC)

Differential scanning calorimeter was performed using a Perkin-Elmer DSC 822e under N_2 atmosphere. The sample was heated from 30 °C to 200 °C at heating rate of 10 °C/min and held at 200 °C for 2 min and then cooled down to 30 °C at heating rate of 10 °C/min (1^{st} run). After that, they were reheated up to 200 °C under the same conditions (2^{nd} run). The crystallization temperature (T_c) of each specimen was recorded from the first run while its melting temperature (T_m) was collected from the second run.

6.3.9.4 Thermogravimetric Analysis (TGA)

The samples were analyzed by TGA using a Perkin-Elmer Pyris Diamond TG/DTA instrument under N_2 flow of 200 ml/min. The heating process was conducted from 30 to 900°C at a rate of 10°C/min.

6.4 Results and discussion

6.4.1 Morphological study by FE-SEM

The clay dispersion into PP matrix was investigated by an FE-SEM in the Figure 6.1 and 6.2. These figures show the SEM micrographs of the cryogenic-fractured surface of all the nanocomposite films with concentration of 1 wt% of nanoclay at different magnifications (1000X and 4500X). The white spots in the Si-mappings referred to the silicate dispersion in the nanocomposites. The Figure 6.1 and 6.2 illustrated a uniform dispersion of clay platelets in PP matrix could be clearly observed. Additionally, with two steps of the melt mixing of PP matrix and modified nanoclay, the high rotational speed during melt blending induced double processes and shear stress bringing about the good dispersion of the clay in the PP matrix, suggested by Chafidz *et al.* (2012).

The morphological study of PP nanocomposite films was determined by an SEM in the Figure 6.3. These figures showed the SEM micrographs of the cryogenic-fractured surface at 10k of magnification of neat PP film compared to those of all the nanocomposite films with concentration of 1 wt% of nanoclay and

with different contents of silver nanoparticles. In case of the nanocomposite films, the inorganic particles were quite homogeneously dispersed in the PP matrix because the fractured surface revealed the absence of clay aggregates. The clay was dispersed in such a way that the layered silicates were completely surrounded by the PP matrix, which implied the good adhesion between the PP chains and layered silicates, observed by the harmonically blended interface of both the PP matrix and clay particles. Yuan and Tian suggested that the good interfacial interactions implied the mineral domains were submicron in size and each lamella of MMT had been dispersed well in polymer matrix. In this research, the good interfacial adhesion resulted from the plasma-based process after the step of masterbatch preparation had been carried out. However, there are certain small voids uniformly presented in the cryogenic-fractured image of cross-sectional surface of PP nanocomposite film (PPBEN) compared to the neat PP; whereas, PPS5BEN, PPS10BEN, PPS15BEN, PPS20BEN showed the bigger voids. In case of Yuan and Tian, they found the pore around 10 microns in a polymer-clay nanocomposite film because of the solvent evaporation, prepared by *in-situ* polymerization and such pores affected the performance of mechanical properties. In our research, the possible reason might originate from the blown film process. In terms of limited mechanical properties, the presence of the γ-Methacryloxypropyltrimethoxysilane-modified silver nanoparticles-loaded bentonite (MSBEN) had a detrimental effect on the elongation at break (Figure 6.5). During the blown film process, if the nanocomposite film was over drawn out, the polymer matrix area near clay particles, which was the rigid location, would be more expanded than other points. The overexpanded area left certain askew and distorted voids at their interface. Another possible reason was that there were a few inorganic tactoids remaining in the PP matrix, causing the void formation. Dumont *et al.* argued that the formation of voids was caused by the insufficiency of interactions between the PP chains and excess inorganic tactoids, which might stir up the voids in the structure of nanocomposites which boosted the gas diffusivity that would be discussed in the next chapter (Chapter VII).

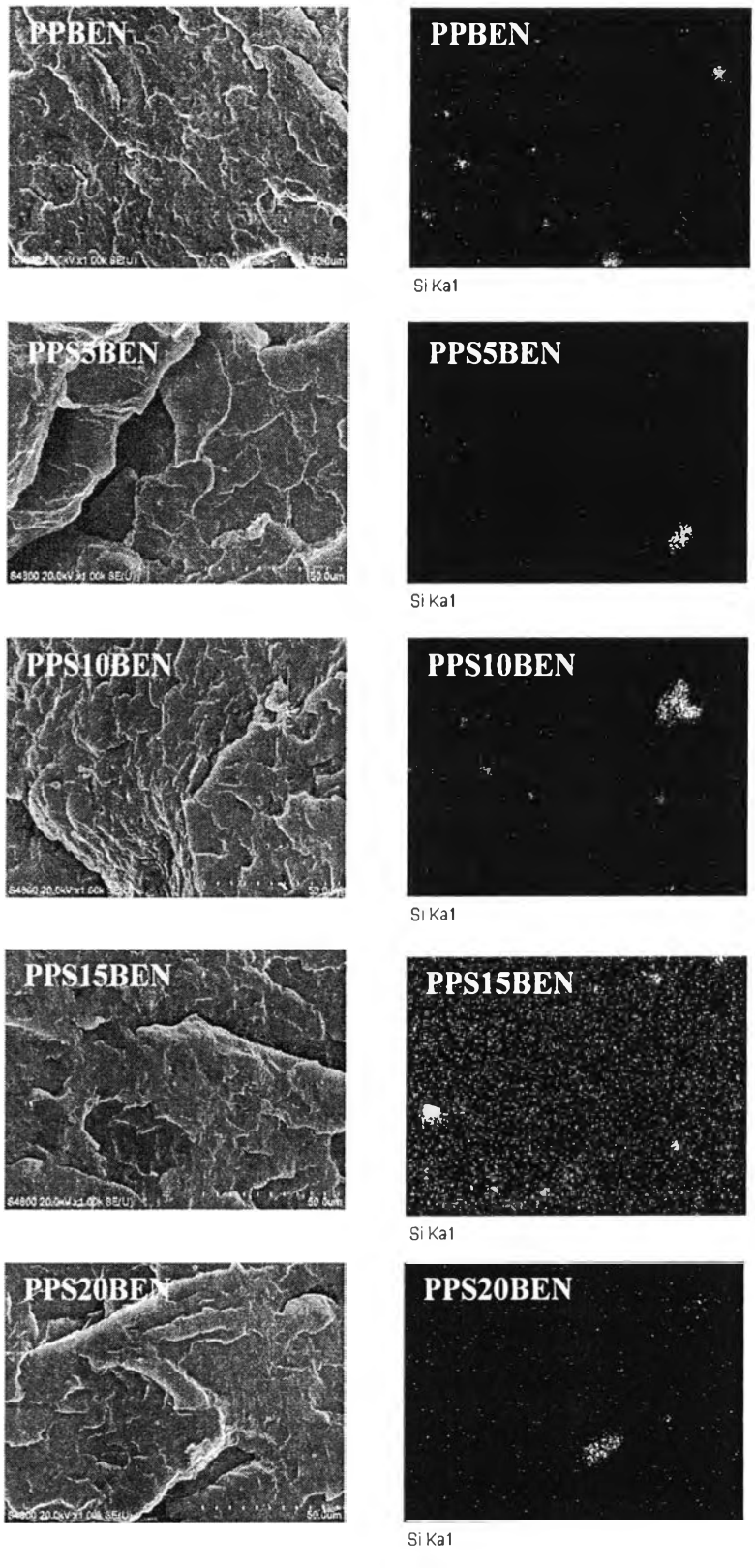

Figure 6.1 Cryogenic-fractured SEM micrographs and Si-mapping of PP-clay nanocomposite blown extrudates (magnification of 1000x).

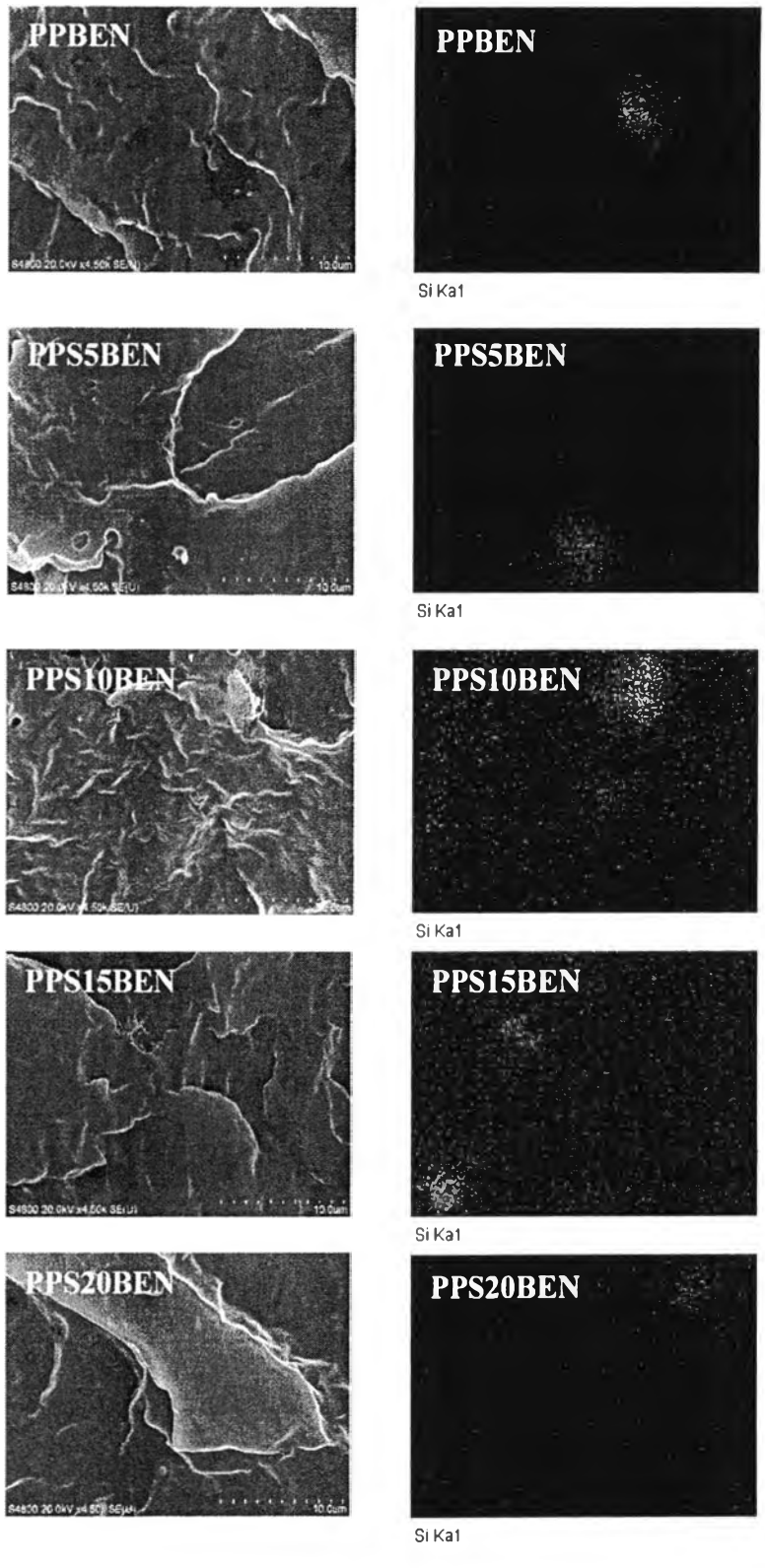

Figure 6.2 Cryogenic-fractured SEM micrographs and Si-mapping of PP-clay nanocomposite blown extrudates (magnification of 4500x).

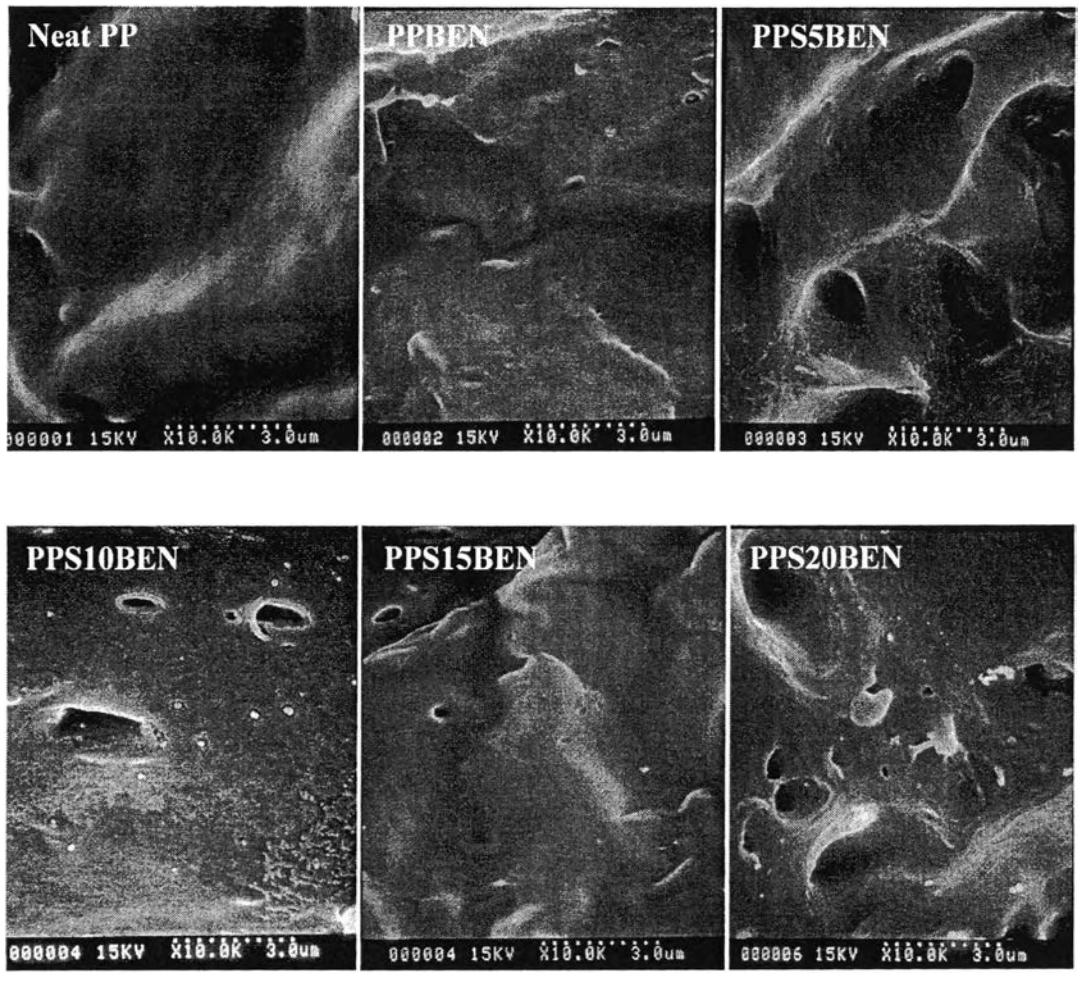

Figure 6.3 Cryogenic-fractured SEM micrographs of PP-clay nanocomposite blown films (magnification of 10,000x).

6.4.2 Mechanical properties of PP-clay nanocompsite films

Table 6.1 and Table 6.2 show all mechanical properties of nanocompsite blown films in both machine (MD) and transverse directions (TD). The mechanical properties of PP nanocomposite films compared to the neat PP were shown in Figure 6.5, 6.6 and 6.7. Generally, the addition of rigid particles into polymers brings about the increasing of tensile strength, tensile modulus, and causes a decrease in elongation at break (Ansari and Ismail, 2008).

In this study, for the MD test, the PPBEN showed no significant increase in tensile strength, but a considerable increase in the percentage of elongation at break by 145 %, compared to neat PP film. Nevertheless, the tensile strength of PPBEN was much higher than that of PPBEN in the TD direction, approximately 18 %, suggesting that the main arrangement of MBEN was in the MD alignment. In the presence of silver nanoparticles, the results showed that their tensile strength and % elongation at break dramatically decreased in the case of PP nanocomposite films compared to neat PP. Tensile strength reduced because the nanocomposites lost their ability to transfer stress during the extension of blown films. The occurrence could be due to some degrees of inhomogeneous fillers acting as stress concentrators to initiate the crack and propagation. Meanwhile, the modified clay and these nanoparticles possibly obstructed the movement of PP chains along applied force with regard to decreased % elongation at break. Although the good distribution and dispersion of layered silicates were achieved as observed by FE-SEM and degree of exfoliation was reached as shown by XRD patterns, certain voids around some dispersed phases were obvious implying the poor adhesion between PP and silicate (Nanoraksa, 2012 and Seephueng, 2008).

For the TD test, in the case of PPBEN and the presence of silver nanoparticles in the films, their %elongation at break had no significant change compared to neat PP. In the case of the films with added silver nanoparticles, they exhibited a slight increase in tensile strength than those of neat PP and the nanocomposite films in the MD test. This possibly due to the the nanoparticles mainly align in TD direction. Nonetheless, the Young's modulus of nanocomposite films (Table 6.1 and 6.2) increased compared to PP films for both of the MD and TD

directions, affected by the presence of silver nanoparticles. The phenomena indicated the higher stiffness of silicate layers originating from the advantageous nano-dispersion of high-aspect-ratio inorganic filler in the nanocompsite films compared to neat PP films.

Table 6.1 Mechanical properties (Machine Direction)

Sample	Young's modulus (GPa)	Tensile strength at yield (MPa)	%Elongation at break (%)
Neat PP	1.15 (0.30)	38.60 (2.46)	303.48 (17.58)[a]
PPBEN	0.89 (0.04)	30.30 (1.42)	743.94 (27.51)
PPS5BEN	1.68 (0.97)	29.92 (2.35)	75.25 (9.89)
PPS10BEN	1.33 (0.16)	33.88 (4.77)	82.10 (2.82)
PPS15BEN	1.85 (0.33)	39.04 (8.68)	75.40 (2.74)
PPS20BEN	1.36 (0.12)	37.69 (5.46)	33.41 (4.60)

[a] the number in parentheses refered to standard deviation

Table 6.2 Mechanical properties (Transverse Direction)

Sample	Young's modulus (GPa)	Tensile strength at yield (MPa)	%Elongation at break (%)
Neat PP	1.23 (0.09)	23.34 (3.69)	4.79 (0.31)[a]
PPBEN	1.35 (0.24)	29.76 (2.41)	10.60 (0.22)
PPS5BEN	1.51 (0.37)	30.85 (0.39)	9.90 (2.65)
PPS10BEN	1.28 (0.17)	30.35 (1.43)	13.29 (0.63)
PPS15BEN	1.60 (0.22)	25.47 (2.65)	3.75 (0.69)
PPS20BEN	1.29 (0.45)	23.97 (0.47)	5.98 (0.73)

[a] the number in parentheses refered to standard deviation

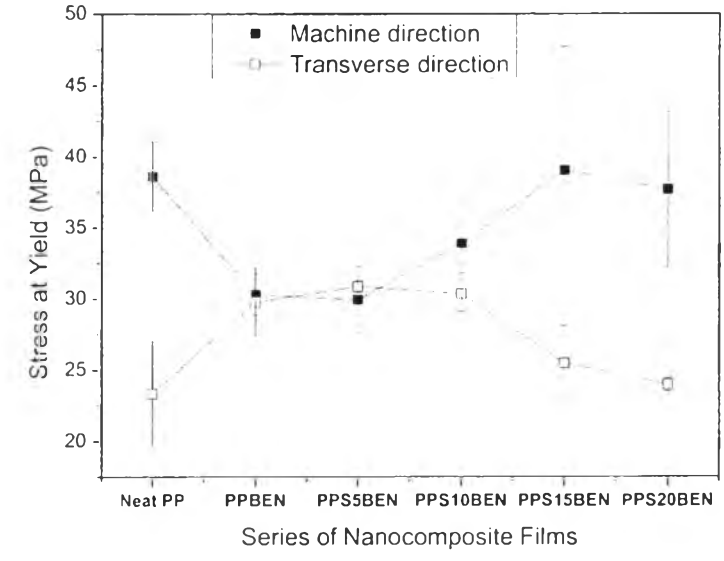

Figure 6.4 Tensile strength at yield of neat PP and PP nanocomposite films.

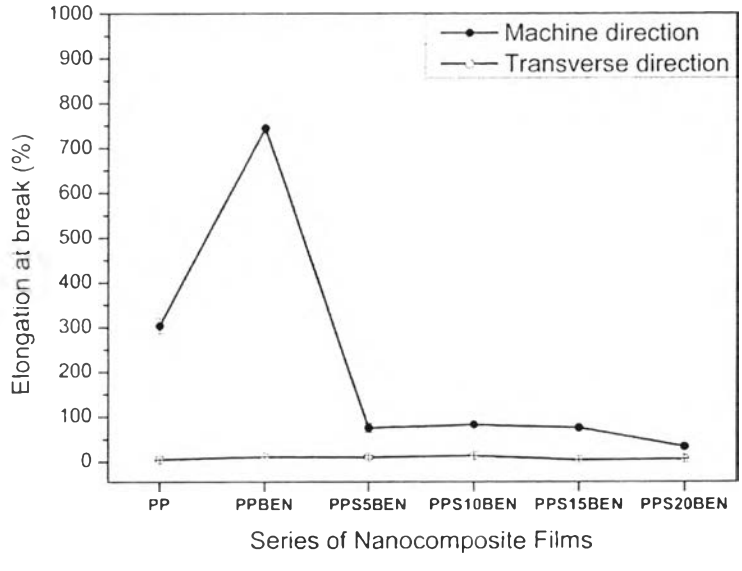

Figure 6.5 Percentage of elongation at break of neat PP and PP nanocomposite films.

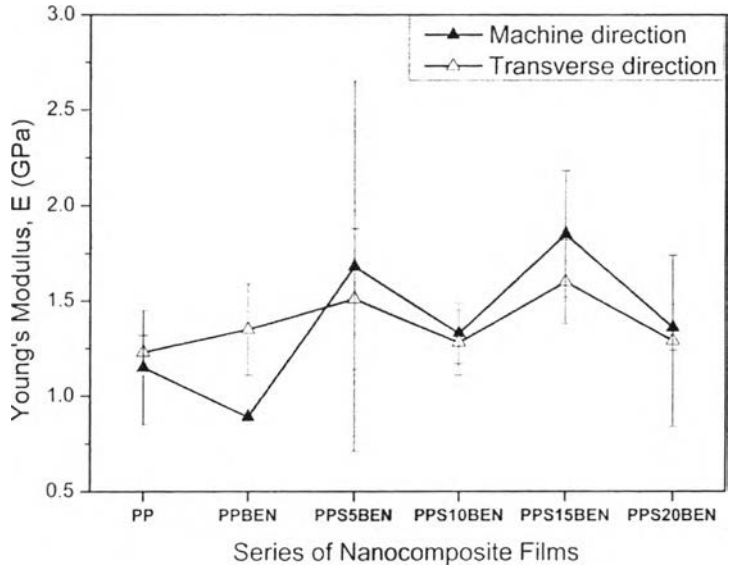

Figure 6.6 Young's modulus of neat PP and PP nanocomposite films.

6.4.3 Crystallization and melting behaviors of PP-clay nanocomposite films

Crystallization and melting behaviors of PP-clay nanocomposite films was measured by a DSC. The DSC thermograms are shown in the Figure 6.6 and Figure 6.7. The Table 6.3 revealed that after the addition of modified clay and silver nanoparticles in the PP nanocomposite films, the crystallization temperature (T_c) and melting temperature (T_m) and percentage of crystallinity (χ_c) were likely to increase as a result of the bentonite and nanoparticles acting as the nucleating agent for the crystallization of PP (Nancraksa, 2012 and Seephueng, 2008). Moreover, it was noticeable that the percentage of crystallinity (χ_c) of the PP nanocomposite films increased with increasing contents of silver nanoparticles. In other word, the silver nanoparticles also performed as a nucleating agent.

Table 6.3 Melting and crystallization behavior of neat PP and PP-clay nanocomposite films

Sample	T_c (°C)	T_m (°C)	ΔH_m (J/g)	χ_c [a] (%)
Neat PP	114.8	161.2	89.3	43.14
PPBEN	115.7	164.0	97.9	47.31
PPS5BEN	116.9	164.6	101.4	48.99
PPS10BEN	118.2	162.8	102.4	49.49
PPS15BEN	116.5	164.2	102.5	49.54
PPS20BEN	117.2	163.4	103.1	49.83

100% crystallinity of PP, ΔH_m^0 = 209 J/g (Bahrami and Mirzaie, 2011)

[a] For the crystallinity of the nanocomposite films, $\chi_c = \frac{\Delta H_m / \emptyset}{\Delta H_m^0} \times 100$

where ΔH_m is the melting enthalpy of the PP and its nanocomposite films,

ΔH_m^0 is the melting enthalpy of 100% crystalline PP,

and $\emptyset$ is the mass ratio of PP in the PP nanocomposite films.

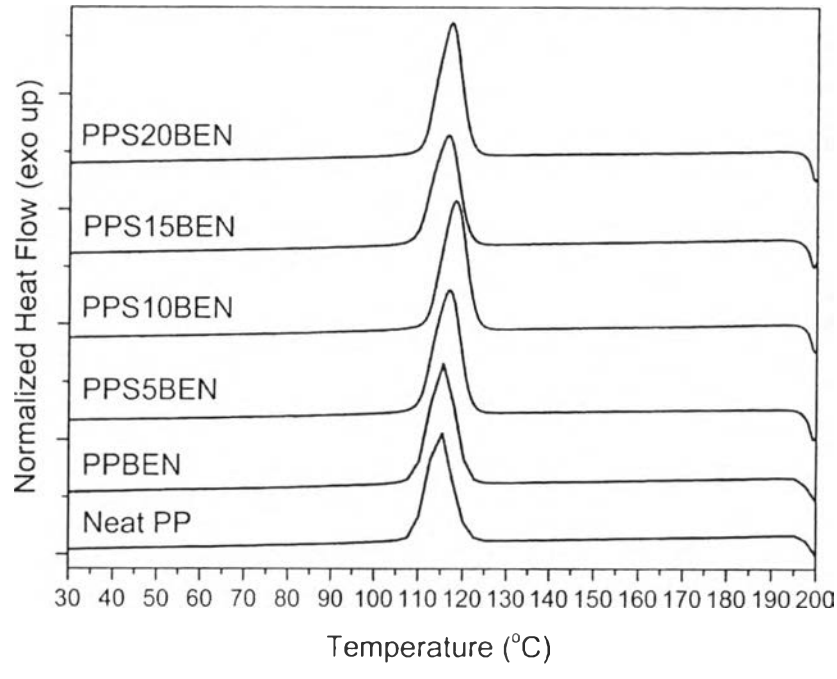

Figure 6.7 Crystallization temperature of neat PP and PP nanocomposite films.

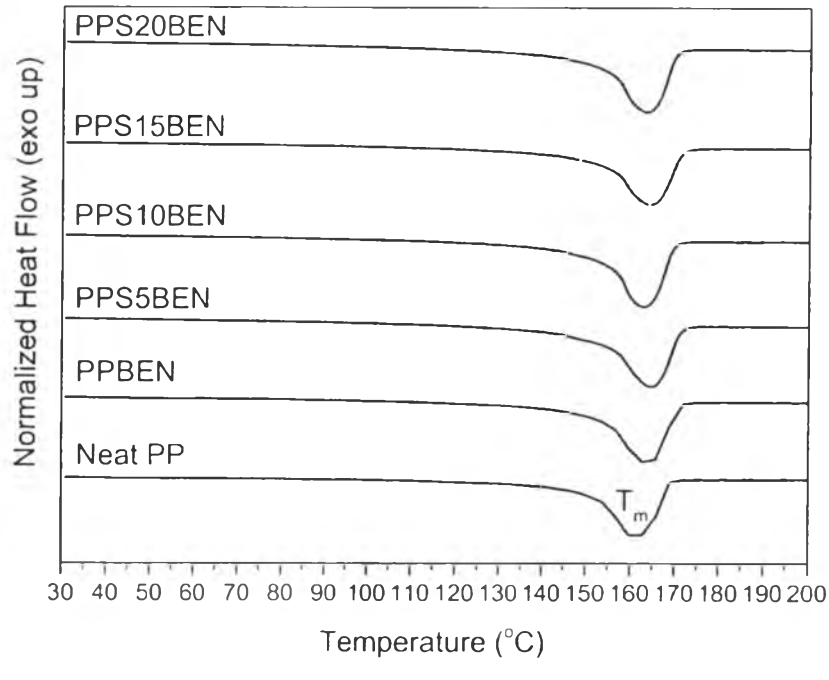

Figure 6.8 Melting temperature of neat PP and PP nanocomposite films.

6.4.4 Crystal structure of PP-clay nanocomposite films

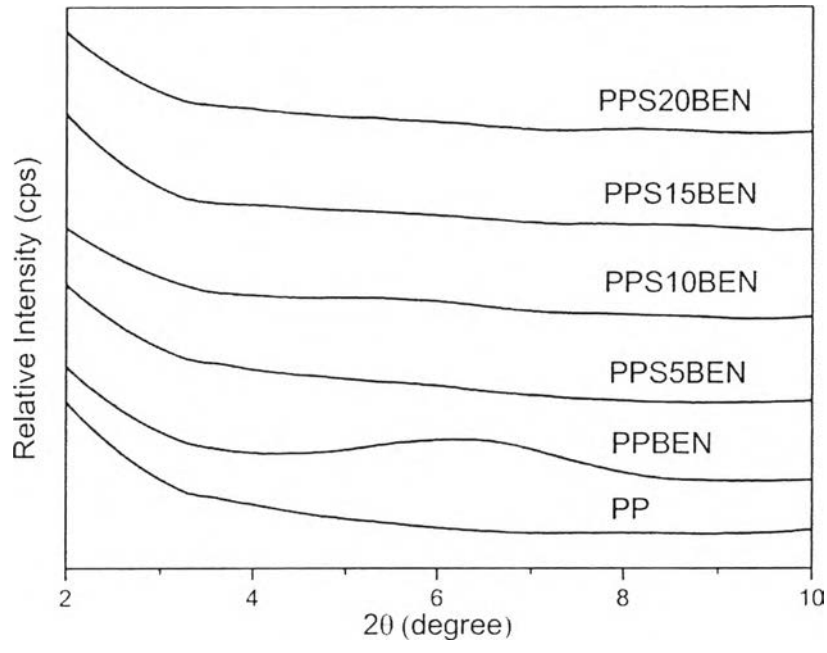

Figure 6.9 SAXD patterns of virgin PP and its nanocomposite blown films pointing out certain levels of intercalated and exfoliated structures of nanoclay in the material.

In order to confirm the formation of intercalated and/or exfoliated nanocomposites, the SAXD analysis was performed as stated ealier. The Figure 6.2 depicts the XRD diffragtograms for the nanocomposite films. In the case of PPBEN, a shift of 2-theta angle to lower degree was congruent with an increase in d-spacing of layered silicates through the expansion of clay layers in PP-modified clay nanocomposite films. With the addition of silver nanoparticles in the interlayer of the silicates, it promoted the diffusion of the polymer into the interlayers of bentonite because at 1 wt% addition of clay, it was obviously speculated that the low angle peak was dissapear resulting from the good delamination and better dispersion of layered silicates in the PP matrix consistent with the Si-mapping from the FE-SEM/EDS analysis. The result corresponds with the explanation as described by Villaluenga *et al.* (2007). The researcher explained that when d_{001} in the PP-clay nanocomposites was higher than in the pure clay alone, it suggested that the

polypropylene molecules were positioned between the interlayers of clay and an intercalated nanocomposite is hence produced. Furthermore, if the peak of d_{001} is not observed in the diffractograms of the nanocomposites, it was concluded that there were enough polypropylene chains, which were inserted into the intergalleries of layered silicates giving rise to the formation of a nanocomposite with an exfoliated structure where the polymer chains were nanoscopically confined.

6.4.5 Thermal stability

Thermal stability of all nanocomposite films was measured by TGA. TGA curves are shown in the Figure 6.9. This Figure and Table 6.4 obviously revealed that the onset decomposition temperatures of the nanocomposite films were higher than that of neat PP film because of the presence of metal oxides including the silver nanoparticles in the modified bentonite such as silica, aluminium, and magnesium, as mentioned in Chapter IV (Xie *et al.*, 2010; Varothai *et al.*, 2007). Evidently, at 2 %wt. loss, the all the PPSBEN films showed a noticeable increase in T_d than those of the PPBEN and neat films due to silver nanoparticles could retard the degradation of the nanocomposite films at elevated temperature. For example, in the case of PPS20BEN, it showed an increase by approximately 20 °C and 14 °C compared to neat PP and PPBEN film, respectively. This result agrees with a research on PP-organoclay nanocomposite films containing copper nanoparticles from Naneruksa (2012). The researcher remarked that high heat capacity of nanoparticles could absorb much heat in the vicinity. Therefore, the PP molecules in those films degraded at higher temperature.

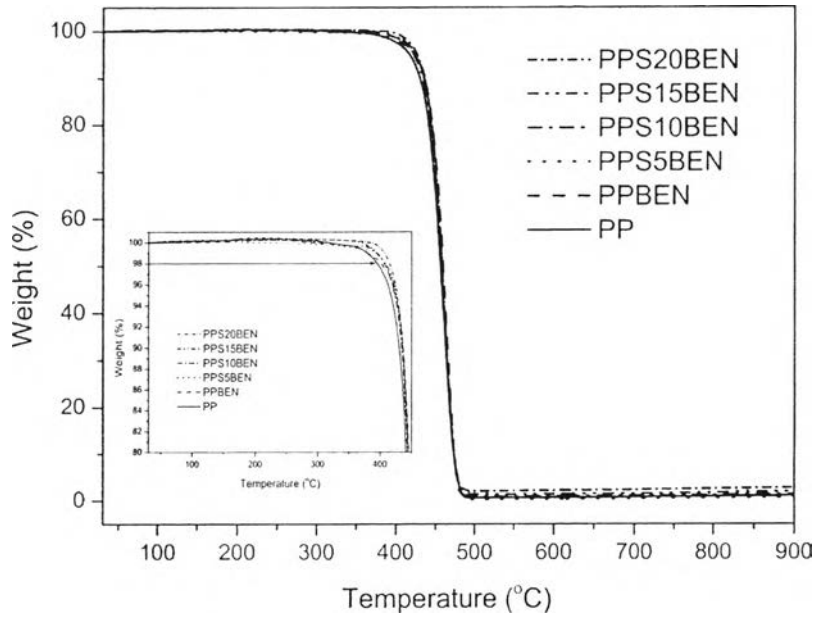

Figure 6.10 Thermogravimetric analysis thermograms of PP and its nanocomposites.

Table 6.4 Thermal behavior of neat PP and PP-clay nanocomposite films

Materials	T_d onset (°C)	T_d at 2%wt loss (°C)	Char Residue (%)
PP	437.2	395.7	-
PPBEN	442.1	401.6	0.9
PPS5BEN	439.9	408.8	0.5
PPS10BEN	439.3	406.6	0.9
PPS15BEN	441.1	408.3	1.1
PPS20BEN	441.7	415.0	1.7

6.5 Conclusions

Blown PP nanocomposites with 1 wt% of clay films consisting different contents of silver nanoparticles (5, 10, 15, and 20 wt% in the clay) were prepared. Finally, the nanocomposites were blown to a clear film for packaging application. PP-clay nanocomposites with 1 wt% nanoclay showed intercalated and exfoliated structures observed by XRD. FE-SEM showed a good distribution and dispersion of modified clay in the PP matrix originating from the double melt-mixing process. For mechanical properties, an increase in the Young's modulus indicating the higher stiffness of the nanocomposite films was reported, although the intercalated and partly exfoliated nanocomposite films had a detrimental effect on the tensile strength and the percentage of elongation at break resulting from the inhomogeneous aggregates and some voids around dispersed phase. As for the DSC analysis, it was found that crystallization temperature, melting temperature, and % crystallinity increase due to nucleating effect of modified clay. Evidently, from TGA analysis at 2 wt% loss, it was clearly shown that 20 wt% of silver nanoparticle film exhibited higher decomposition temperature than neat PP film approximately 20 °C.

6.6 Acknowledgement

This work was financial supported by the Higher Education Research Promotion and National Research University Project of Thailand, Office of the Higher Education Commission (FW0649A). The author is grateful for chemicals and the laboratory equipment support from Polymer Processing and Polymer Nanomaterials Research Unit, The Petroleum and Petrochemical College, Chulalongkorn University.

6.7 References

Appendini, P., Hotchkiss, J.H. (2002) Review of Antimicrobial Food Packaging. Innovative Food Science & Emerging Technologies, 3, 113-126.

Azizi, H., Morshedian, J., Barikani, M., Wagner, M.H. (2010) Effect of Layered Silicate Nanoclay on the Properties of Silane Crosslinked Linear Low-Density Polyethylene (LLDPE). eXPRESS Polymer Letters, 4, 252–262.

Chafidz, A., Ali, I., Ali Mohsin, M. E., Elleithy, R., Al-Zahrani, S. (2012) Nanoidentation and Dynamic Mechanical Properties of PP/Clay Nanocomposites. Journal of Polymer Research, 19, 1-12.

Cooksey, K. (2005) Effectiveness of Antimicrobial Food Packaging Materials. Food Additives and Contaminants, 22, 980-987.

Dumont, M.-J., Reyna-Valencia, A., Emond, J.-P., Bousmina, M. (2006) Barrier Properties of Polypropylene/Organoclay Nanocomposites. Journal of Applied Polymer Science, 103, 618-625.

El-Kheshen, A. A., Gad El-Rab, S.F. (2012) Effect of reducing and protecting agents on size of silver nanoparticles and their anti-bacterial activity. Der Pharma Chemica, 4, 53-65.

Hajir Bahrami, S., Mirzaie, Z. (2011) Polypropylene/Modified Nanoclay Composite-Processing and Dyeability Properties. World Applied Sciences Journal, 13, 493-501.

Lamsal, K., Kim, S.W., Jung, J.H., Kim, Y.S., Kim, K.S., Lee, Y.S. (2011) Application of Silver Nanoparticles for the Control of *Colletotrichum* Species *In Vitro* and Pepper Anthracnose Disease in Field. The Koren Society of Mycology, 3, 194-199.

Maria, A. D., Aurora, A., Montone, A., Tapfer, L., Pesce, E., Balboni, R., Schwarz, M., Borriello, C. (2011) Synthesis and Characterization of PMMA/Silylated MMTs. Journal of Nanoparticle Research, 13, 6049-6058.

Nasrollahi, A., Pourshamsian, Kh., Mansourkiaee, P. (2011) Antifungal Activity of Silver Nanoparticles on Some of Fungi. International Journal of Nano Dimension (IJND), 3, 233-239.

Naneraksa, P. (2012) Smart Packaging from Plastic/Nanocopper Nanocomposite. M.S. Thesis, The Petroleum and Petrochemical College, Chulalongkorn University, Bangkok, Thailand.

Seephueng, A. (2008) Smart Packaging for Fish Spoilage Indicator. M.S. Thesis, The Petroleum and Petrochemical College, Chulalongkorn University, Bangkok, Thailand.

Sharma, S. K., Nayak, S.K. (2009) Surface Modified Clay/Polypropylene (PP) Nanocomposites: Effect on Physico-Mechanical, Thermal and Morphological Properties. Polymer Degradation and Stability, 94, 132-138.

Tang, Y., Hu, Y., Song, L., Zong, R., Gui, Z., Chen, Z., Fan, W. (2003) Preparation and Thermal Stability of Polypropylene/Montmorillonite Nanocomposites. Polymer Degradation and Stability, 82, 127–131.

Varothai, Y. (2007) Active Packaging Based on Ethylene Scavenger PP/Organomodified Clay Nanocomposites. M.S. Thesis, The Petroleum and Petrochemical College, Chulalongkorn University, Bangkok, Thailand.

Villaluenga, J.P.G., Khayet, M., Lo´pez-Manchado, M.A., Valentin, J.L., Seoane, B., Mengual, J.I. (2007) Gas Transport Properties of Polypropylene/Clay Composite Membranes. European Polymer Journal: Macromolecular Nanotechnology 43, 1132-1143.

Xie, Y., Hill, C.A.S., Xiao, Z., Militz, H., Mai, C. (2010) Silane Coupling Agents Used for Natural Fiber/Polymer Composites: A Review. Composites Part A: Applied Science and Manufacturing, 41, 806-819.

Yuan, X., Tian, Z. (2010), Effect of Ultrasonic on the Properties of Silicone/ Montmorillonite Nanocomposites by *in-situ* Intercalative Polymerization. Advanced Materials Letters, 1, 135-142.